JOURNAL OF BACTERIOLOGY, June 1996, p. 3025–3030 Vol. 178, No. 11
0021-9193/96/$04.00+0

Conformational Change of the Hexagonally Packed Intermediate Layer of *Deinococcus radiodurans* Monitored by Atomic Force Microscopy

DANIEL J. MÜLLER,[1,2] WOLFGANG BAUMEISTER,[3] AND ANDREAS ENGEL[2]*

M. E. Müller-Institute for Microscopic Structural Biology, Biozentrum, University of Basel, CH-4056 Basel, Switzerland,[1] and IBI-2:Structural Biology, Forschungszentrum Jülich, D-52425 Jülich,[2] and Max-Planck-Institut für Biochemie, D-82152 Martinsried bei München,[3] Germany

Received 11 January 1996/Accepted 26 March 1996

Both surfaces of the hexagonally packed intermediate (HPI) layer of *Deinococcus radiodurans* were imaged in buffer solution by atomic force microscopy. When adsorbed to freshly cleaved mica, the hydrophilic outer surface of the HPI layer was attached to the substrate and the hydrophobic inner surface was exposed to the stylus. The height of a single HPI layer was 7.0 nm, while overlapping edges of adjacent single layers adsorbed to mica had a height of 14.7 nm. However, double-layered stacks with inner surfaces facing each other exhibited a height of 17.4 nm. These stacks exposed the outer surface to the stylus. The different heights of overlapping layers and stacks are attributed to differences in the interaction between inner and outer surfaces. At high resolution, the inner surface revealed a protruding core with a central pore connected by six emanating arms. The pores exhibited two conformations, one with and the other without a central plug. Individual pores were observed to switch from one state to the other.

Nearly all archaebacterial cell envelopes incorporate a regular surface layer (S layer) of protein or glycoprotein subunits (17). S layers are also widely distributed among eubacteria but less ubiquitously than among archaebacteria (3, 25). Electron microscopy has served as the major tool to elucidate their architecture and assembly (4, 26). Accounting for 7 to 12% of the total cell protein, S layers are expected to be a vital interface between the cell and its environment (5). Thus, they are supposed to protect the cell from hostile factors and to serve as molecular sieves for the uptake of nutrients and release of metabolites. Other functions may involve the determination of cell shape, cell-cell recognition, cell-cell communication, and cell adhesion, but none of these has been unambiguously established (for recent reviews, see references 3, 24, and 25).

One extensively studied S layer is the hexagonally packed intermediate (HPI) layer, which represents the major cell envelope protein of the radiotolerant bacterium *Deinococcus radiodurans* (2). It is released from the underlying outer membrane by the extraction of whole cells with detergent (2) and can thus be isolated efficiently. The HPI layer has been characterized biochemically (2), by electron microscopy (1, 21, 30), by scanning tunneling microscopy (11, 27, 29), and by atomic force microscopy (13, 14). Assembled from one protein (M_r of 107,028 [20]) forming hexamers with an M_r of 655,000 (9), the HPI layer lattice has a unit cell size of 18 nm. One hexagonal unit is composed of a massive core from which spokes that connect adjacent units emanate. According to the three-dimensional model from electron microscopy (1), this core encloses a pore and is surrounded by six relatively large openings centered about the three-fold axis.

The atomic force microscope (AFM) (6) has the potential to contour the topography of biological macromolecules in their native environment (8). Developments in specimen preparation techniques and technical improvements in AFM hardware and cantilever fabrication have allowed several membrane proteins to be imaged at high resolution (7, 12, 13, 31). To validate the structural details determined with the AFM, topographs have been compared with data from both electron microscopy (14, 19) and X-ray crystallography (23). While these comparisons demonstrate the high level of accuracy of the surface contour with the AFM, it has been shown that the AFM is also capable of monitoring dynamic processes (8). This capability suggests that it should be possible to study structural changes of proteins with the AFM and to relate them to the function of the particular protein. However, such experiments require imaging at vertical forces of approximately 0.1 nN, since the structure of proteins can be reversibly changed by the imaging process (18). Exploiting this novel imaging method to the fullest extent, we demonstrate here that the HPI layer has an inner surface with two distinct conformations.

MATERIALS AND METHODS

Specimen preparation. HPI layer was extracted from whole cells (strain SARK) with lithium dodecyl sulfate and purified on a Percoll density gradient (2). A stock solution (1 mg of protein per ml) in distilled water was diluted to 20 μg/ml in 10 mM Tris-HCl (pH 8.2)–100 mM KCl–20 mM $MgCl_2$ and deposited on freshly cleaved mica. After an adsorption time of 60 min at room temperature, the sample was washed to remove any layers that were not attached firmly to the substrate.

Atomic force microscopy. A Nanoscope III AFM (Digital Instruments, Santa Barbara, Calif.) was used, equipped with a 120-μm scanner and a liquid cell. Oxide-sharpened Si_3N_4 cantilevers with a length of 100 μm (K = 0.38 N/m) and 200 μm (K = 0.06 N/m) were purchased from Digital Instruments. Alternatively, contamination tips were produced in a field emission scanning electron microscope (Hitachi model S-800) (16). To prevent charging, the cantilevers were coated with an approximately 15- to 20-nm thick Au layer. The carbon tips were deposited onto the apex of the Au layer covering the stylus. The field emission scanning electron microscope was operated at the smallest working distance (5 nm) and optimum focus. To minimize the tip radii, the smallest spot size (≈20 Å [2 nm]) was used. The beam was positioned over the stylus at a magnification of 50,000 and kept fixed for 2 min. As a result of the Au layer, the cantilevers had a slightly enhanced spring constant K of approximately 0.15 N/m.

After thermal relaxation for approximately 30 min after a new sample or a new cantilever was mounted, initial engagement of the tip was performed by setting the scan size to zero to minimize specimen deformation or tip contamination.

* Corresponding author. Mailing address: M. E. Müller Institute, Biozentrum, University of Basel, Klingelbergstr. 70, CH-4056 Basel, Switzerland. Phone: 41-61-267-22-61. Fax: 41-61-267-22-59. Electronic mail address: AENGEL@UBACLU.UNIBAS.CH.

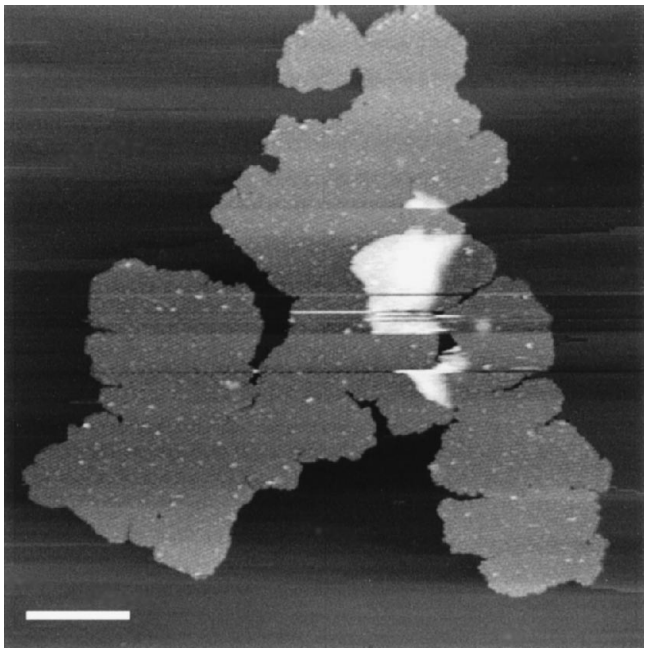

FIG. 1. HPI layer adsorbed to mica in buffer solution. Membranes (20 μg/ml) suspended in 100 mM KCl–20 mM $MgCl_2$–10 mM Tris (pH 8.2) were adsorbed to freshly cleaved mica for 60 min and subsequently washed to remove membranes that were not firmly adsorbed. The image was recorded with an oxide-sharpened Si_3N_4 stylus at a force of approximately 100 pN with a scan speed of 4 μm/s. Scale bar, 500 nm.

Before the surfaces were scanned, force-distance curves were determined, and the operating point of the microscope was set to a force less than 1 nN. Images were obtained simultaneously in trace and retrace directions, with a force of <0.2 nN applied to the stylus. During scanning, the applied force was corrected manually to compensate for the thermal drift of the instrument.

Height measurements. The calibration of the scanner was carried out as described previously (19). Sheets of HPI layers and purple membranes were adsorbed simultaneously to freshly cleaved mica in buffer solution (10 mM Tris-HCl [pH 8.2], 150 mM KCl). The heights of single HPI layers, stacks, and overlapping sheets were compared directly with the height of the purple membrane. As reported previously (19), the purple membrane showed a height of 5.6 ± 0.2 nm at pH 8.2.

Image processing. Images (512 by 512 pixel) were transferred to a Vax 3100 workstation. They were flattened line by line, and correlation averages were produced by using a reference unit cell taken from the raw data with the Semper image processing system (22). Single particle averaging and classification were accomplished as described previously (10).

RESULTS

Figure 1 shows a typical overview of a large HPI layer fragment adsorbed to freshly cleaved mica in Tris-KCl buffer. Flat sheets with diameters of up to 5 μm were firmly attached to the substrate and remained stable during several hours of scanning at vertical forces of <0.2 nN.

While most of the membranes were adsorbed as single layers, the formation of stacks was also observed. All HPI layers studied (n = 120) were attached with their outer surfaces facing the mica. If the HPI layers formed stacks, the lower first layer (Fig. 2a, right) exposed its inner surface to the stylus. The second layer (Fig. 2a, center) was directed with its inner surface towards the lower layer and thus exposed its outer surface to the stylus. The upper layer (Fig. 2a, left) of the stack (n = 3) exposed its inner surface to the stylus and, therefore, had its outer surface facing the outer surface of the layer below (Fig. 2b). The average height of the HPI layer relative to the substrate was 7.0 ± 0.5 nm (n = 91), whereas double-layer stacks exhibited a height of 17.4 ± 0.8 nm (n = 10). When two layers adsorbed to mica overlapped, the measured height was 14.7 ± 0.5 nm (n = 15).

High-resolution images. Because of the preferential adsorption of the HPI layer, the outer surface could be imaged only when a double layer was formed. In Fig. 3a, a high-resolution topograph obtained from such a stack shows the fine structure of the outer surface, which does not exhibit interferences from the lower layer and which is in excellent agreement with previous results (13, 14) displayed in Fig. 3c and d. Six protomers form the core with a central pore, arranged in a hexagonal lattice (a = b = 18 ± 0.4 nm). To enhance the signal-to-noise ratio, correlation averages (n = 10) were calculated and symmetrized sixfold (Fig. 3b). The V-shaped protrusions of protomers are clearly visible (compare Fig. 3b and d). These domains were arranged on an equilateral hexagon with a side length of 4.9 ± 0.2 nm. The height difference between the V-shaped protrusion and the emanating arms was 1.2 ± 0.2 nm, while the maximum height of the protrusions was 2.2 ± 0.7 nm.

Figure 4a presents the submolecular details of the inner surface. The connecting arms emanating from adjacent cores are clearly visible, even before image averaging. Pores appear to exist in two different conformations. While some individual pores showed a central depression (white circles), others showed a single protrusion located at the center (white squares). When the same HPI molecules were imaged after 5 min (Fig. 4b), some initially open pores were closed (white circles), while some initially closed ones were open (white squares). The central protrusion of the closed conformation seemed to be less distinct than the surrounding core.

To analyze the structural differences, 330 units from 10 dif-

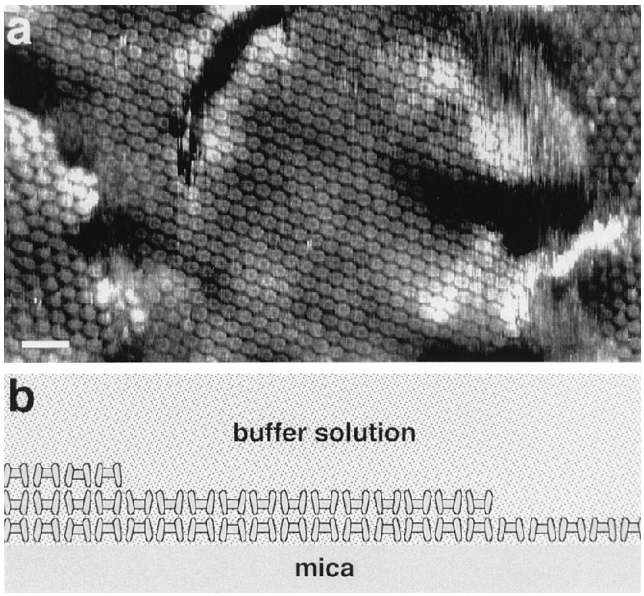

FIG. 2. (a) A three-layered stack of HPI layers adsorbed to mica. (b) As schematically drawn the outer surface of the lowest layer was attached to mica, while the inner surfaces of the lowest and middle layers were attached to one another. Thus, the inner membrane surface of the lowest layer and the outer membrane surface of the middle layer were directed towards the stylus. The inner surface of the top layer is again exposed towards the stylus, because the top layer adsorbed with its outer surface to the middle layer. The imaging conditions were pH 8.2 (100 mM KCl, 10 mM Tris), an oxide-sharpened Si_3N_4 stylus, a scan frequency of 3.6 Hz (scan speed of 1.45 μm/s), and an imaging force of approximately 100 pN. (a) Scale bar, 50 nm.

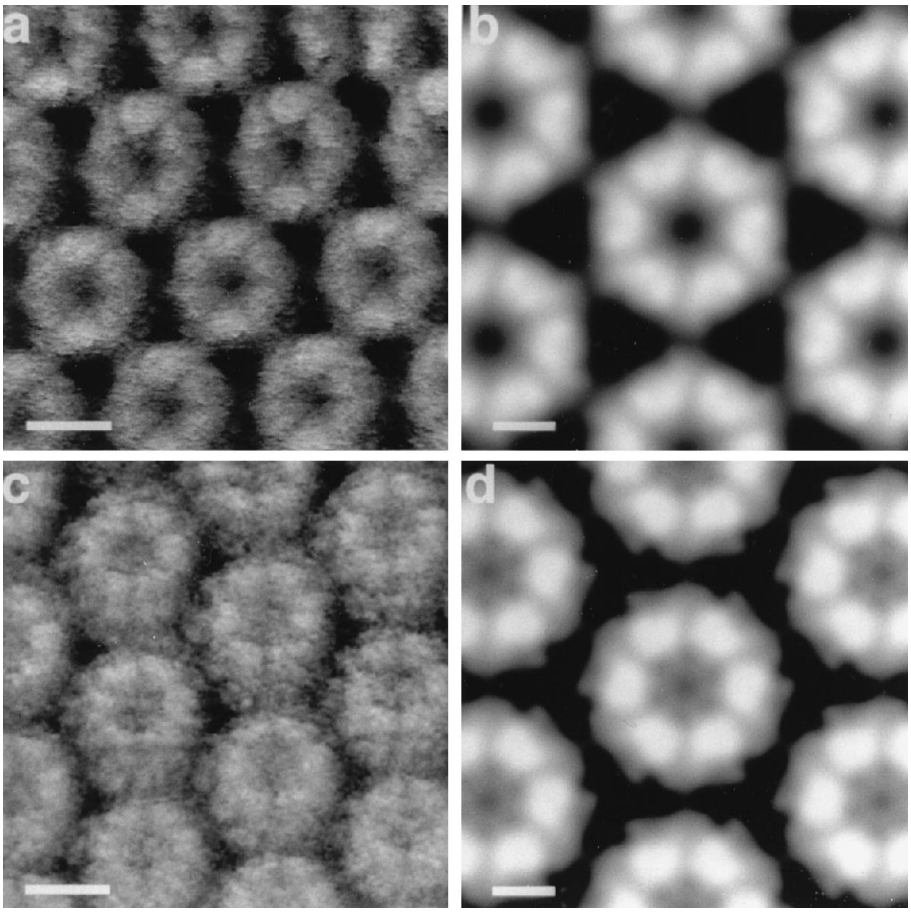

FIG. 3. High-resolution scan of outer surface of HPI. (a) The donut-like structure of the core with six V-shaped protrusions and six spokes is distinct. The averaged and sixfold symmetrized topograph was calculated from 10 unit cells. (b) The root mean square deviation from sixfold symmetry was 14.4%. (c) Raw data of a single HPI layer photocross-linked to silanized glass. (d) Correlation average of 50 unit cells (14). The full grey level range corresponds to 6 nm (a and c) and 2 nm (b and d) of vertical distance. The imaging conditions used were pH 8.2 (100 mM KCl, 20 mM $MgCl_2$, 10 mM Tris), an oxide-sharpened Si_3N_4 stylus, a scan frequency of 2.35 Hz (scan speed of 153 nm/s), and an imaging force of approximately 100 pN. Scale bars, 10 (a and c) and 5 (b and d) nm.

ferent images were translationally and angularly aligned and subjected to multivariate statistical analysis (10, 28). A total of 265 units partitioned into two classes from which the class averages were calculated (Fig. 4c and d). The average in Fig. 4c shows six subunits, with a seventh protrusion located at the center of the pore, whereas the average in Fig. 4d exhibits a unit with an open pore. The difference map displayed in Fig. 4g between these two conformations was calculated after sixfold symmetrization of the averages (Fig. 4e and f). The prominent difference was located at the center of the core, and the six protrusions forming the core appear to have shifted slightly towards the center during the switch from a closed state (Fig. 4e) to an open state (Fig. 4f). In the open conformation (Fig. 4f), the depression of the core was 1.8 ± 0.5 nm, whereas the depression over the protrusion of the closed conformation (Fig. 4e) was 1.0 ± 0.5 nm.

Figure 5a shows the topography of the inner surface recorded with an electron beam deposited carbon supertip. The montage in Fig. 5b was calculated from sixfold symmetrized correlation averages of either open or closed conformations. The six protrusions of the core were arranged on an equilateral hexagon with a side length of 4.0 ± 0.2 nm. The height difference between protrusions and spokes was 2.5 ± 0.2 nm, while the total height of the protrusions was 2.9 ± 0.3 nm.

DISCUSSION

In Tris buffer (10 mM Tris-HCl [pH 8.2], 100 to 200 mM KCl) HPI layers adsorbed firmly to freshly cleaved mica in a preferential orientation. This pattern is due to the different properties of the outer and the inner surfaces. The inner surface, which interacts with the outer membrane, has a hydrophobic anchor while the outer surface is hydrophilic (1). Thus, only the hydrophilic outer surface adsorbs to the freshly cleaved mica surface. In contrast, when immobilized by photocross-linking to activated glass plates, exclusively the hydrophobic inner surface was attached to the substrate, because the glass surfaces were hydrophobic after chemical modification (13).

If HPI layers formed stacks, it was found that either hydrophobic or hydrophilic surfaces were in contact, hence exposing the outer surface to the stylus when the stack contained an even number of layers (Fig. 2). Single layers exhibited a thickness of 7.0 ± 0.5 nm. As shown in Table 1, this value compares favorably with results from scanning transmission electron microscopy and transmission electron microscopy of freeze-dried samples. Height values for single layers determined by different methods on different substrates vary between 3.7 and 8.2 nm. The scanning tunneling microscopic measurements of air-

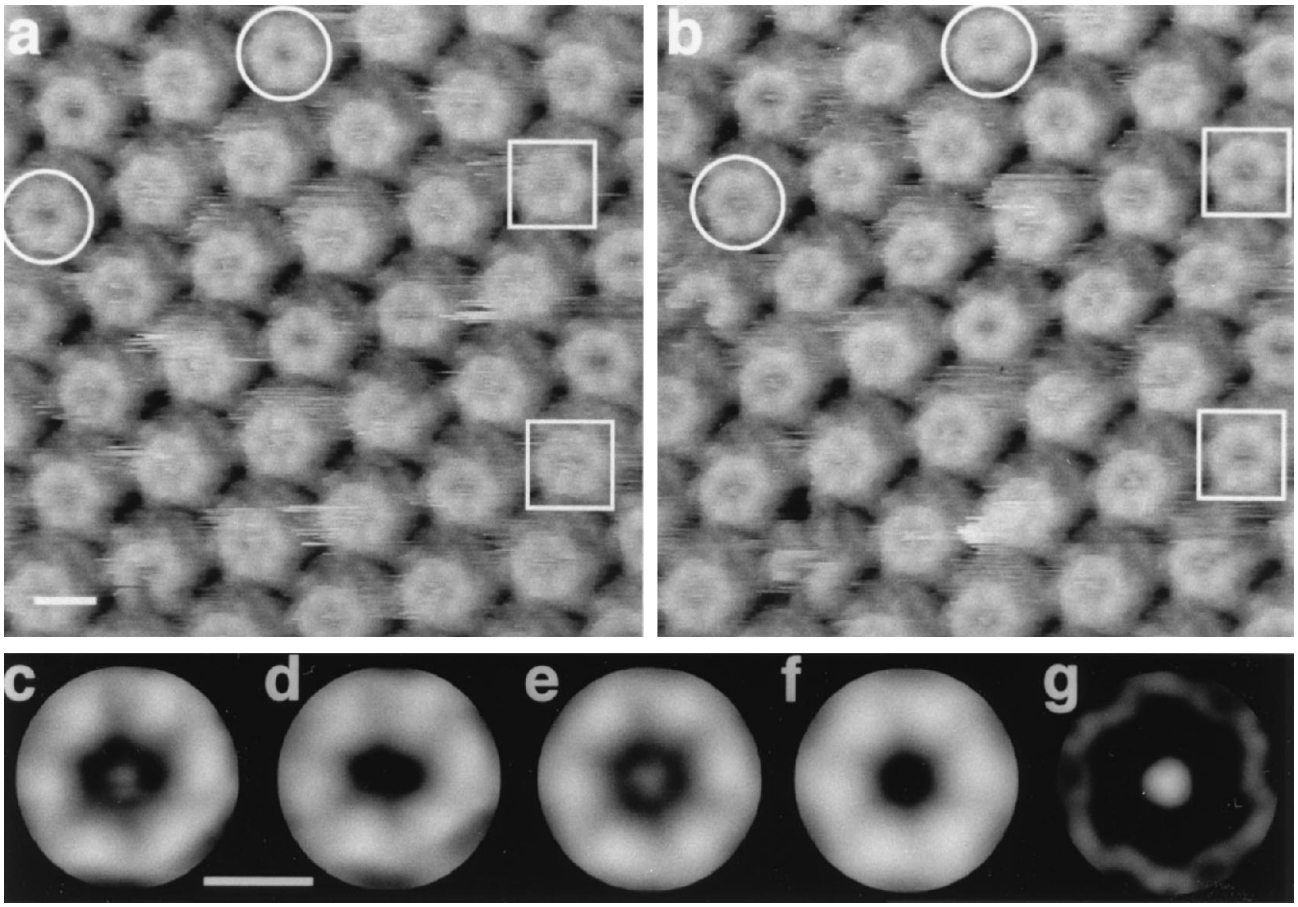

FIG. 4. Conformational changes of inner surface of HPI layer. (a) The protruding cores are clearly visible, with some pores in an open conformation and others in an obstructed conformation. (b) Area shown in panel a imaged 5 min later. Some pores which were open earlier are now closed (circles), while closed ones have opened during this time interval (squares). Units were aligned and classified into two classes (see the text). The class averages exhibit a plugged (c) and an open hexamer (d). The difference map (g) represents the modulus of the height difference between the sixfold-symmetrized class averages (e and f). The full grey level range corresponds to a vertical distance of 6 (a and b) and 3 (c to f) nm. The imaging conditions, pH 8.2 (100 mM KCl, 20 mM $MgCl_2$, 10 mM Tris), an oxide-sharpened Si_3N_4 stylus, a scan frequency of 1.97 Hz (scan speed of 270 nm/s), and an imaging force of 100 pN, were kept constant throughout the observation. Scale bars, 10 (a and b) and 6 (c to g) nm (raw data and averaged data, respectively).

dried, metal-coated HPI layers provided the lowest values (27, 29), while transmission electron microscopic measurements of freeze-dried, metal-shadowed single HPI layers or thin-sectioned HPI layer stacks gave the highest ones (30).

The difference in height between air-dried and freeze-dried or native HPI layer (imaged in buffer solution) is significant. This difference is attributed to the flattening of the HPI layer during dehydration in air (1, 15). In addition, as the hydrophilic outer surface adsorbs strongly to the hydrophilic carbon film, it could be deformed by interface forces (1, 15). It is likely that this deformation is promoted by surface tension forces during dehydration in air. Denaturation of the surface facing the solid support might also influence the structure of the opposite surface of a single HPI layer. However, as demonstrated in Fig. 3, we could not detect structural differences between the outer surfaces to a resolution of 1.5 nm when HPI layers were observed as single layers immobilized by photocross-linking on glass (14) or as stacks adsorbed to mica.

Overlapping layers exhibited a thickness of 14.7 ± 0.5 nm, in excellent agreement with the single-layer height of 7.0 ± 0.5 nm. In contrast, the height of stacks formed when inner surfaces were in contact with each other was approximately 3 nm larger than expected (17.4 ± 0.8 nm). This has reproducibly been observed for different types of tips and at forces of <0.2 nN. Similar values had previously been measured on thin sections of stacks (17.2 ± 1.2 nm; [30]) and with the AFM in buffer solution (17.4 ± 0.5 nm [13]). Therefore, we conclude that the interaction between the inner and outer surfaces of the HPI layer differs drastically from the interaction between two inner surfaces, the latter probably involving the hydrophobic anchors that are thought to mediate the attachment of the HPI layer to the outer membrane (1).

The inner surface of the HPI layer exhibited two conformations (Fig. 5), which we refer to as open and closed because the central pore of the hexameric core was unobstructed in one case and plugged in the other case. The three-dimensional map of negatively stained HPI layer indicates the presence of a small plug about the sixfold axis (1). As demonstrated here, the AFM allows the switching between these states to be monitored. It is not known what induces the switching, and tip-induced conformational changes appear to be plausible. However, we have used hydrophilic oxide-sharpened Si_3N_4 tips as well as hydrophobic carbon contamination tips to observe the same topography of the inner surface and the same random switching behavior. In addition, we have operated the AFM at vertical forces below 0.2 nN while scanning the protein

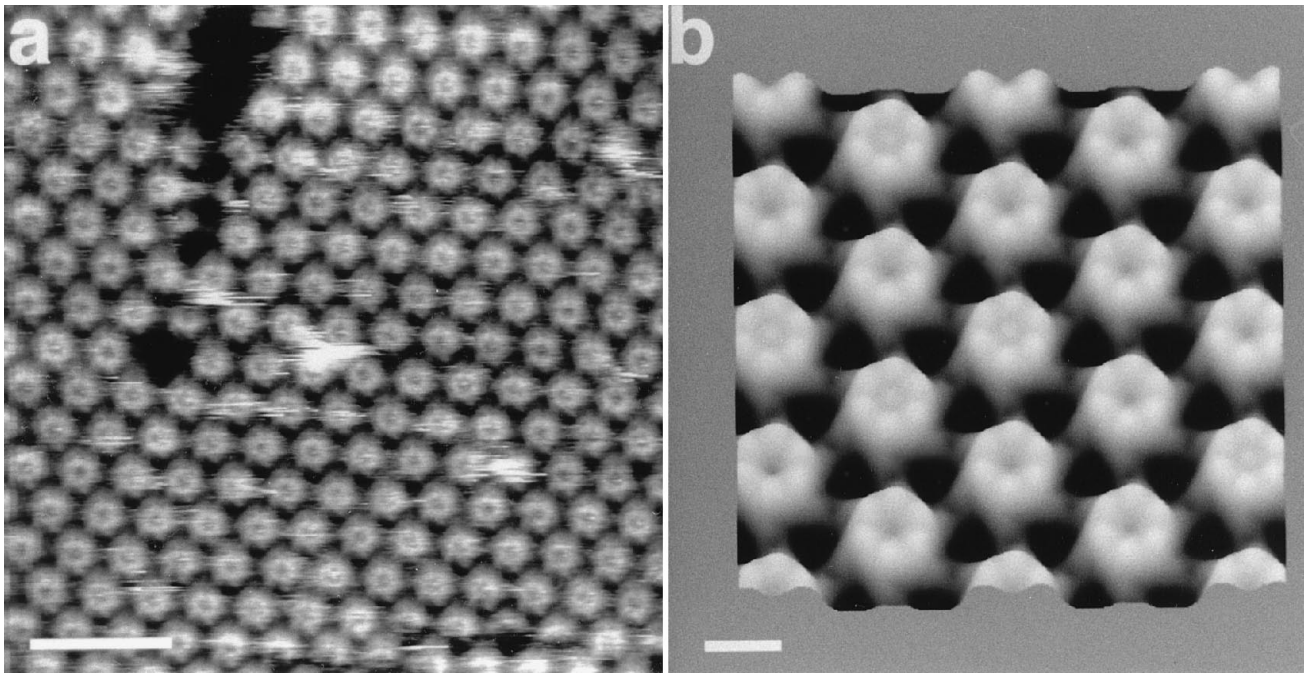

FIG. 5. Image of inner HPI layer acquired in buffer solution with an electron beam deposited carbon superstylus at a vertical force of <0.2 nN. (a) As also shown in Fig. 4, open and closed pores coexist. (b) Sixfold-symmetrized correlation averages of both open and closed conformations were assembled in a montage of the bacterial surface layer. The distinct arms emanating from the cores of the hexamers exhibit an anticlockwise rotation. The root-mean-square deviation from sixfold symmetry was 7.2%. The full grey level range of the average corresponds to 3 nm of vertical distance. The imaging conditions used were pH 8.2 (100 mM KCl, 20 mM $MgCl_2$, 10 mM Tris), a scan frequency of 1.97 Hz (scan speed of 600 nm/s), and an imaging force of 150 pN. Scale bars, 50 (a) and 10 (b) nm.

surfaces at high magnification. Tip-induced conformational changes of a single polypeptide loop connecting the bacteriorhodopsin helices E and F require forces larger than 0.2 nN (18). As a result of the rigorous isolation protocol involving extensive detergent extraction, it can be ruled out that significant contaminants are present (2). Taken together, it is likely that the observed random switching between open and closed states is a specific property of the HPI layer. Electron microscopy data to a resolution of 0.83 nm have suggested that the central channel has a diameter of 2.2 nm (21), allowing passage of molecules up to 5 kDa at any time. If the HPI layer indeed serves as protective coat, it is conceivable that the observed open and closed states of the central pore are biologically relevant.

TABLE 1. Thickness or height of HPI layers

Preparation	Method[a]	Layer thickness or height (nm)[b]	Reference
Freeze-dried	STEM	6.9 ± 0.5	9
Freeze-dried, metal shadowed	TEM	8.2 ± 1.0	30
	STM	5.1,[c] 4.8 ± 0.5[d]	29
Air-dried, metal shadowed	TEM	7.0 ± 1.0	30
	STM	(3.8–4.6)[e] ± 0.2	29
	STM	5.7 ± 0.5	27
Freeze-fracturing	TEM	7.7 ± 1.0	30
Thin sections of stacks	TEM	8.6 ± 0.6	30
Physiological buffer, cross-linking	AFM	6.6 ± 0.5	13
		17.2 ± 1.4 (double layer)	
Physiological buffer	AFM	7.0 ± 0.5	This work
		17.4 ± 0.8 (double layer)	
		14.7 ± 0.5 (overlapping layer)	

[a] STEM, scanning transmission electron microscopy; TEM, transmission electron microscopy; STM, scanning tunneling microscopy; AFM, atomic force microscopy.
[b] Single-layer height unless otherwise specified.
[c] Outer surface up.
[d] Inner surface up.
[e] Variations depend on orientation and preparation protocol.

Conclusion. The AFM enables not only the possibility of imaging the surfaces of biological systems at high resolution but also new possibilities of directly monitoring conformational changes of individual molecules. Although no physiological data that correlate with the observed conformational changes are currently available, the results presented here might stimulate further studies of the function of the HPI layer in particular and bacterial surface layers in general.

ACKNOWLEDGMENTS

This work was supported by the Swiss National Foundation for Scientific Research (grant no. 31-42435.94 to A.E.), the Deutsche Forschungsgemeinschaft (SFB 189 to D.J.M.), and the Maurice E. Müller Foundation of Switzerland.

We are indebted to A. Heft for producing the carbon supertips.

REFERENCES

1. **Baumeister, W., M. Barth, R. Hegerl, R. Guckenberger, M. Hahn, and W. O. Saxton.** 1986. Three-dimensional structure of the regular surface layer (HPI layer) of *Deinococcus radiodurans*. J. Mol. Biol. **187:**241–253.
2. **Baumeister, W., F. Karrenberg, R. Rachel, A. Engel, B. Ten Heggeler, and W. O. Saxton.** 1982. The major cell envelope protein of *Micrococcus radiodurans* (R1). Eur. J. Biochem. **125:**535–544.
3. **Baumeister, W., I. Wildhaber, and H. Engelhardt.** 1988. Bacterial surface proteins: some structural, functional and evolutionary aspects. Biophys. Chem. **29:**39–49.
4. **Baumeister, W., I. Wildhaber, and B. M. Phipps.** 1989. Principles of organization in eubacterial and archaebacterial surface proteins. Can. J. Microbiol. **35:**215–227.
5. **Beveridge, T. J.** 1981. Ultrastructure, chemistry, and function of the bacterial wall. Int. Rev. Cytol. **72:**229–317.
6. **Binnig, G., C. F. Quate, and C. Gerber.** 1986. Atomic force microscope. Phys. Rev. Lett. **56:**930–933.
7. **Butt, H.-J., K. H. Downing, and P. K. Hansma.** 1990. Imaging the membrane protein bacteriorhodopsin with the atomic force microscope. Biophys. J. **58:**1473–1480.
8. **Drake, B., C. B. Prater, A. L. Weisenhorn, S. A. C. Gould, T. R. Albrecht, C. F. Quate, D. S. Cannell, H. G. Hansma, and P. K. Hansma.** 1989. Imaging crystals, polymers, and processes in water with the atomic force microscope. Science **243:**1586–1588.
9. **Engel, A., W. Baumeister, and W. Saxton.** 1982. Mass mapping of a protein complex with the scanning transmission electron microscope. Proc. Natl. Acad. Sci. USA **79:**4050–4054.
10. **Frank, J., J.-P. Bretaudiere, J.-M. Carazo, A. Veschoor, and T. Wagenknecht.** 1987. Classification of images of biomolecular assemblies: a study of ribosomes and ribosomal subunits of *Escherichia coli*. J. Microsc. **150:**99–115.
11. **Guckenberger, R., W. Wiegräbe, A. Hillebrand, T. Hartman, Z. Wang, and W. Baumeister.** 1989. Scanning tunneling microscopy of a hydrated bacterial surface protein. Ultramicroscopy **31:**327–332.
12. **Hoh, J. H., G. E. Sosinsky, J.-P. Revel, and P. K. Hansma.** 1993. Structure of the extracellular surface of the gap junction by atomic force microscopy. Biophys. J. **65:**149–163.
13. **Karrasch, S., M. Dolder, J. Hoh, F. Schabert, J. Ramsden, and A. Engel.** 1993. Covalent binding of biological samples to solid supports for scanning probe microscopy in buffer solution. Biophys. J. **65:**2437–2446.
14. **Karrasch, S., R. Hegerl, J. Hoh, W. Baumeister, and A. Engel.** 1994. Atomic force microscopy produces faithful high-resolution images of protein surfaces in an aqueous environment. Proc. Natl. Acad. Sci. USA **91:**836–838.
15. **Kellenberger, E., M. Häner, and M. Wurtz.** 1982. The wrapping phenomenon in airdried and negatively stained preparations. Ultramicroscopy **9:**139–150.
16. **Keller, D., and C. Chih-Chung.** 1992. Imaging step, high structures by scanning force microscopy with electron beam deposited tips. Surface Sci. **268:** 333–339.
17. **König, H.** 1988. Archaebacterial cell envelopes. Can. J. Microbiol. **34:**395–406.
18. **Müller, D. J., G. Büldt, and A. Engel.** 1995. Force-induced conformational change of bacteriorhodopsin. J. Mol. Biol. **249:**239–243.
19. **Müller, D. J., F. A. Schabert, G. Büldt, and A. Engel.** 1995. Imaging purple membranes in aqueous solutions at subnanometer resolution by atomic force microscopy. Biophys. J. **68:**1681–1686.
20. **Peters, J., M. Peters, F. Lottspeich, W. Schäfer, and W. Baumeister.** 1987. Nucleotide sequence of the gene encoding the *Deinococcus radiodurans* surface protein, derived amino acid sequence, and complementary protein chemical studies. J. Bacteriol. **169:**5216–5223.
21. **Rachel, R., U. Jakubowski, H. Tietz, R. Hegerl, and W. Baumeister.** 1986. Projected structure of the surface protein of *Deinococcus radiodurans* determined to 8 Å resolution by cryomicroscopy. Ultramicroscopy **20:**305–316.
22. **Saxton, W. O., T. J. Pitt, and M. Horner.** 1979. Digital image processing: the semper system. Ultramicroscopy **4:**343–354.
23. **Schabert, F. A., C. Henn, and A. Engel.** 1995. Native *Escherichia coli* OmpF porin surfaces probed by the atomic force microscopy. Science **268:**92–94.
24. **Sleytr, U. B., and P. Messner.** 1983. Crystalline surface layers on bacteria. Annu. Rev. Microbiol. **37:**311–339.
25. **Sleytr, U. B., and P. Messner.** 1988. Crystalline surface layers in prokaryotes. J. Bacteriol. **170:**2891–2897.
26. **Sleytr, U. B., and P. Messner.** 1989. Self-assembly of crystalline bacterial cell surface layers (S-layers), p. 14–31. *In* H. Plattner (ed.), Electron microscopy of subcellular dynamics. CRC Press, Boca Raton, Fla.
27. **Stemmer, A., R. Reichelt, R. Wyss, and A. Engel.** 1991. Biological structures imaged in a hybrid scanning transmission electron microscope and scanning tunneling microscope. Ultramicroscopy **35:**255–264.
28. **van Heel, M.** 1984. Multivariate statistical classification of noise images (randomly orientated biological macromolecules). Ultramicroscopy **13:**165–184.
29. **Wang, Z., T. Hartman, W. Baumeister, and R. Guckenberger.** 1990. Thickness determination of biological samples with a z-calibrated scanning tunneling microscope. Proc. Natl. Acad. Sci. USA **87:**9343–9347.
30. **Wildhaber, I., H. Gross, A. Engel, and W. Baumeister.** 1985. The effects of air-drying and freeze-drying of the structure of a regular protein layer. Ultramicroscopy **16:**411–422.
31. **Yang, J., J. X. Mou, and Z. F. Shao.** 1994. Molecular resolution atomic force microscopy of soluble proteins in solution. Biochim. Biophys. Acta **1199:** 105–114.